Non-local approach to kinetic effects on parallel transport in fluid models of the scrape-off layer

John Omotani and Ben Dudson

York Plasma Institute, Department of Physics, University of York, Heslington, York, YO10 5DD, UK

Email: john.omotani@york.ac.uk

Abstract

By using a non-local model, fluid simulations can capture kinetic effects in the parallel electron heat-flux better than is possible using flux limiters in the usual diffusive models. Non-local and diffusive models are compared using a test case representative of an ELM crash in the JET SOL, simulated in one dimension. The non-local model shows substantially enhanced electron temperature gradients, which cannot be achieved using a flux limiter. The performance of the implementation, in the BOUT++ framework, is also analysed to demonstrate its suitability for application in three-dimensional simulations of turbulent transport in the SOL.

The divertor target heat-flux will be an important limit on the performance of future magnetic confinement fusion devices, from ITER onwards[1, 2]. Modelling of transport in the scrape-off layer (SOL) is therefore a subject of urgent interest. The conditions in the SOL—large amplitude fluctuations, open magnetic field lines—prevent the application of approximations that are used to make (gyro-)kinetic simulations of turbulence feasible in the core plasma; kinetic simulations are limited to one-dimensional models (e.g. [3]). Nevertheless, three-dimensional features—turbulence and 'blob'[4] motion—are critical parts of the picture, especially in determining the width of the scrape-off layer[5, 6]. These are studied using fluid simulations which are either two-dimensional (e.g. ESEL[7, 8], RI/FI-SOL[9], SOLT[10] and G-ESEL[11]) or use simple (Braginskii) models for the parallel dynamics (e.g. heat diffusion in GBS[12] or Spitzer conductivity in BOUT++[13, 14]). However, such simple treatments of the parallel transport may not give the full picture. As a consequence of an edge localized mode (ELM) or the motion of a blob through the SOL there will be large changes in the overall density and temperature on a field line. When such transient events occur kinetic simulations show that the diffusive description is not a good model of the parallel transport: the correction for 'kinetic effects' that can be applied by using flux limiters breaks down since the appropriate limiter, as determined by comparison with kinetic simulations, varies strongly in time[15].

To enable a self-consistent treatment of turbulence with 'kinetically-corrected' parallel transport, new methods for including kinetic effects in fluid models are required. This paper describes the application of a non-local calculation of the electron heat-flux[16], which has not previously been applied to the SOL. The parallel electron heat-flux is derived by using a very high order truncation (with typically 100 to 1600 moments retained) to solve a one-dimensional reduced drift kinetic equation in terms of a set of integrals. This model has a couple of particularly attractive features. Firstly, being derived directly from the kinetic equation, it has no ad-hoc parameters. Secondly, a good deal of the computational complexity involved is found in solving for the eigensystem that is used to decouple the moment equations. This need be done only once for a given truncation, and so a substantial piece of the 'kinetic' part of the calculation is removed from the simulations. Alternatives, which have been used in laser-plasma physics[17, 18], employ integral kernels which would be numerically very challenging when, as is the case here, the density cannot be assumed to be constant.

The model has been implemented in the BOUT++ plasma fluid simulation framework[19] in order to expedite its future inclusion in three-dimensional simulations. Here we evaluate its performance through one-dimensional simulations of parallel transport, with parameters chosen to approximate an ELM in JET[20].

In Section 1 we outline the model and detail some additions needed for its use in the SOL; in Section 2 the results of simulations of the test case are presented, comparing the non-local model to the Braginskii model with and without flux limiters; in Section 3 the numerical performance of the implementation is discussed, which is particularly important for future extensions to three-dimensional fluid models; finally in Section 4 we conclude and discuss future developments.

1 Theory

1.1 Non-local heat-flux

The thermal speed of the electrons in SOL plasmas is very much higher than that of the ions. Hence in calculations of the electron dynamics, we may consider the evolution of the background profiles to be slow. Solving a static electron kinetic equation for the heat-flux will therefore give a good approximation to its true value, which can then be used in the evolution equations for the background fields.

The approach taken in [16] starts from the one-dimensional kinetic equation for the non-Maxwellian part δf_e of the electron distribution function whose Maxwellian part is $f_e^{(0)}$:

$$v_{||}\frac{\partial \langle \delta f_e \rangle}{\partial l} = \sum_{a=e,i} C\Big(\langle f_e^{(0)} + \delta f_e \rangle, \langle f_a^{(0)} + \delta f_a \rangle\Big) - v_{||}\frac{\partial \langle f_e^{(0)} \rangle}{\partial l} \tag{1}$$

where $\langle\cdot\rangle$ denotes the gyroaverage, $v_{||}$ is the component of the velocity parallel to the magnetic field and $C\left(\cdot,\cdot\right)$ is the linearized Fokker-Planck collision operator. We expand in fluid moments on a basis $P^{lk}(\mathbf{v}) = P^l(\mathbf{v})L_k^{(l+\frac{1}{2})}(v^2)$, $P^l(\mathbf{v})$ being tensor harmonic polynomials and $L_k^{(l+\frac{1}{2})}(v^2)$ associated Laguerre polynomials (see [21] for details), and truncate to L angular harmonics and K Laguerre orders, i.e. $0 \leq l < L$, $0 \leq k < K$; here we will take $L = 20$, $K = 20$ and so have 400 moments in total. After truncating it is convenient to represent the pairs (l, k) with a single index, $A, B, \ldots$, running over $L \times K$ possible values. Then (1) reduces to a set of one-dimensional, first order ODEs for the non-Maxwellian fluid moments

$$\sum_B \Psi^A{}_B \left(\frac{\partial n^B}{\partial z} - 3n^B \frac{1}{v_{Te}} \frac{\partial v_{Te}}{\partial z}\right) = \sum_B C^A{}_B n^B + g^A \tag{2}$$

where z is the dimensionless length defined by $\frac{\partial z}{\partial l} = \frac{1}{\Lambda_C}$ (with Λ_C the electron-electron collision length); n^A are the parallel fluid moments of f_e; $\Psi^A{}_B$ is the matrix coming from $v_{||}$; $C^A{}_B$ is the collision matrix; and

$$g^A = \frac{5}{4} \frac{n_e}{T_e} \frac{\partial T_e}{\partial z} \delta_{A,(1,1)} \tag{3}$$

is the drive term from the gradient of the Maxwellian part, $f_e^{(0)}$. These equations are valid only for the non-Maxwellian moments (i.e. $A, B = (0, 0), (0, 1)$ and $(1, 0)$ are excluded): the Maxwellian moments (the density, temperature and fluid velocity) are background fields which give the drive term g^A.

The term due to the gradient of the thermal velocity, which was neglected in [16], has been retained; as we will see below it is unimportant for the core plasma, but it becomes relevant in the SOL. The equations (2) can be decoupled using the eigenvectors of the matrix operator $\left(C^{-1}\Psi\right)^A{}_B$ to give

$$\zeta_{(A)} \left(\frac{\partial \hat{n}^A}{\partial z} - 3\hat{n}^A \frac{1}{v_{Te}} \frac{\partial v_{Te}}{\partial z}\right) = \hat{n}^A + \hat{g}^A \tag{4}$$

where $\hat{n}^A$ and $\hat{g}^A$ are the components of n^A and g^A on the eigenvector basis and $\zeta_{(A)}$ are the corresponding eigenvalues (note that as defined here $\zeta_{(A)}$ are the reciprocals of the eigenvalues used in [16][1]). The solutions of these

equations can be expressed as

$$\hat{n}^A(z) = \begin{cases} -\hat{g}^A & \zeta_{(A)} = 0 \\[2mm] \hat{n}^A(z_0)\left(\frac{T(z)}{T(z_0)}\right)^{\frac{3}{2}}\exp\left(\frac{z-z_0}{\zeta_{(A)}}\right) & \\[1mm] +\int_{z_0}^z dz'\left(\frac{T(z)}{T(z')}\right)^{\frac{3}{2}}\exp\left(\frac{z-z'}{\zeta_{(A)}}\right)\frac{\hat{g}^A(z')}{\zeta_{(A)}} & \zeta_{(A)} \neq 0 \end{cases} \tag{5}$$

where $\hat{n}^A(z_0)$ are the values at the boundary z_0 (where $z_0 \equiv z_- < z$ for $\zeta_{(A)} < 0$ and $z_0 \equiv z_+ > z$ for $\zeta_{(A)} > 0$). The $T^{\frac{3}{2}}$ factors result from the $\frac{\partial v_{Te}}{\partial z}$ term. In the core, flux surfaces are closed and so fluctuations in T are small compared to T, thus $\frac{T(z)}{T(z_0)} \approx \frac{T(z)}{T(z')} \approx 1$ and these factors can be neglected (as they are in [16]). In the SOL this is not the case as flux surfaces are open and the change in temperature along a field line may be large.

Finally, after transforming back to the original vector basis we use the $(1,1)$ moment to calculate the parallel heat-flux, which is needed to close the fluid equations:

$$q_{e||} = -\frac{5}{4}v_{Te}T_e n^{(1,1)} = -\frac{5}{4}v_{Te}T_e \sum_B W^{(1,1)}{}_B \hat{n}^B \tag{6}$$

where $W^A{}_B = W^A_{(B)}$ is the matrix formed from the eigenvectors $W_{(B)}$ (whose eigenvalues are $\zeta_{(B)}$).

So to calculate $q_{e||}$ we must (a) compute integrals over z (as many as the number of moments retained) and (b) set the boundary values $\hat{n}^A(z_0)$ (which we will do so as to impose the boundary condition on the heat-flux, Section 1.3).

1.2 Fluid Equations

For our simulations we use the 1d fluid equations, assuming quasineutrality and ambipolarity,

$$\frac{dn}{dt} + n\nabla_{||}V_{||} = S_n \tag{7}$$

$$m_i n \frac{dV_{||}}{dt} = -\nabla_{||}\left(nT_i\right) - \nabla_{||}\pi_{i||} + \nabla_{||}\left(nT_e\right) - m_i V_{||}S_n \tag{8}$$

$$\frac{3}{2}n\frac{dT_i}{dt} + nT_i\nabla_{||}V_{||} = -\nabla_{||}q_{i||} - \pi_{i||}\nabla_{||}V_{||} + \frac{3n\,m_e}{m_i\tau_{ei}}\left(T_e - T_i\right) + S_E - \frac{3}{2}T_i S_n \tag{9}$$

$$\frac{3}{2}n\frac{dT_e}{dt} + nT_e\nabla_{||}V_{||} = -\nabla_{||}q_{e||} + \frac{3n\,m_e}{m_i\tau_{ei}}\left(T_i - T_e\right) + S_E - \frac{3}{2}T_e S_n \tag{10}$$

where $\frac{d}{dt} \equiv \left(\frac{\partial}{\partial t} + V_{||}\nabla_{||}\right)$, S_n is the particle source, S_E is the energy source (which is taken to be equal for electrons and ions) and τ_{ei} is the electron-ion collision time. The equations are closed by specifying $q_{e||}$, $q_{i||}$ and $\pi_{i||}$:

- $q_{e||}$ is given either by the non-local model described above, by the Braginskii diffusion operator $q_{d,e} = -3.16\frac{n_e T_e \tau_{ei}}{m_e}\nabla_{||}T_e$, or by the flux-limited diffusion operator

$$q_{dl,e} = \left(\frac{1}{q_{d,e}} + \frac{1}{\alpha_e q_{fs,e}}\right)^{-1} \tag{11}$$

---

[1] The reason for this discrepancy is that in [16] the eigenvalues of $\left(\Psi^{-1}C\right)^A{}_B$ are found. Due to the block-off-diagonal structure of Ψ, when the three Maxwellian moments are removed the upper-left-most blocks are no longer square, with the result that Ψ is not invertible. The authors of [16] resolved this by changing the truncation to keep three extra moments $(0, K)$, $(0, K+1)$ and $(1, K)$ so that all the blocks of Ψ remain square. C, though, is block-diagonal and so is invertible with or without the extra moments. The eigenvalues and eigenvectors of $\left(C^{-1}\Psi\right)^A{}_B$ can therefore be found in either case, though without the extra moments there will be (exactly one) zero eigenvalue. The approach taken here is thus more flexible. In this paper we do not add the three extra moments, and do have a zero eigenvalue. The effect is to change the response to fluctuations whose wavelength is short enough (compared to the collision length) that the model does not converge. Without a zero eigenvalue the heat-flux due to such fluctuations is anomalously low, while with one it is anomalously high. The latter case may be better behaved if, for instance, numerical noise happened to introduce such short-wavelength fluctuations.
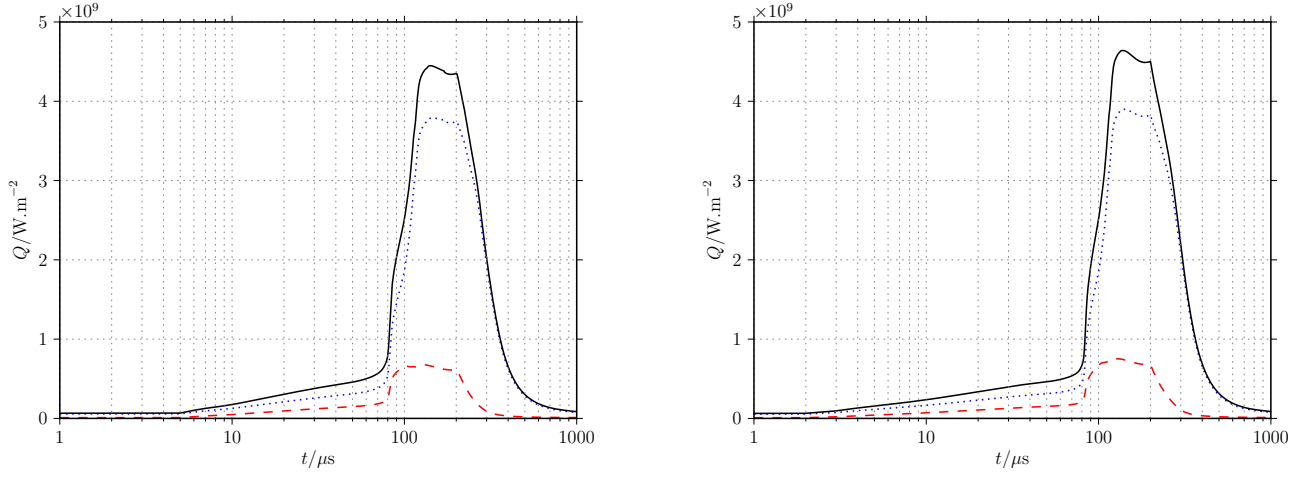
Figure 1: Target heat-flux for simulations using non-local electron heat-flux (left) and unlimited diffusive electron heat-flux (right). The electron component is the red dashed line, the ion component is the blue dotted line and the total is the black solid line. N.B. this is the *target* heat-flux (at the material surface) and not the *sheath-edge* heat-flux that is used as the boundary condition on the fluid model, i.e the electron heat-flux has been shifted down and the ion heat-flux shifted up by the sheath potential. The heat-flux has not, however, been adjusted for the incidence angle at the target, so if the angle were, for instance, $6°$ the true heat-flux at the material surface would be smaller by a factor of ~ 0.1.

where the free-streaming heat-flux is $|q_{fs,e}| = nT_e v_{Te}$ and α_e is a parameter to be set.

- $q_{i||}$ is calculated using a flux-limited diffusion operator

$$q_{i||} = \left(\frac{1}{q_{d,i}} + \frac{1}{\alpha_i q_{fs,i}} \right)^{-1} \tag{12}$$

where the Braginskii diffusion operator is $q_{d,i} = -3.9 \frac{nT_i \sqrt{2} \tau_{ii}}{m_i} \nabla_{||} T_i$, the free-streaming heat-flux is $|q_{fs,i}| = nT_i v_{Ti}$ and α_i is a parameter to be set.

- $\pi_{i||}$ is given by a limited form of the Braginskii viscosity

$$\pi_{i||} = \left(\frac{1}{\pi_0} \pm \frac{1}{bnT_i} \right)^{-1} \equiv \frac{b\pi_0}{\left(\frac{|\pi_0|}{nT_i} + b \right)} \tag{13}$$

where $\pi_0 = -\frac{4}{3} \times 0.96 nT_i \sqrt{2} \tau_{ii} \nabla_{||} V_{||}$ and b is a parameter to be set.

1.3 Boundary Conditions

In the SOL the boundary conditions are a critically important part of the dynamics. Here we wish to impose the sheath-edge fluid boundary conditions[22]

$$V_{se} = \pm c_s = \pm \sqrt{\frac{T_e + \gamma T_i}{m_i}} \tag{14}$$

$$q_{se,e} = (2T_e + |e\phi_s|) nc_s \tag{15}$$

where $e\phi_s = 0.5 T_e \ln \left(2\pi \frac{m_e}{m_i} \left(1 + \frac{\gamma T_i}{T_e} \right) \right)$ is the sheath potential and $\gamma = 3$, representing an approximately collisionless sheath.

(14) and (15) under-determine the boundary values of the non-Maxwellian moments $\hat{n}^A$. Since our aim here is to develop computationally efficient methods to improve fluid turbulence models, we simply choose the boundary

moments so as to impose (15) on the heat-flux and leave the remaining moments unchanged, by adding a contribution proportional to $(W^{-1})^A_{(1,1)}$.

There is an additional complication, that in a hot enough plasma (which is found in the simulations described below) the collision length may be long enough that the transients originating at one boundary do not decay to zero by the time they reach the other. This means that the boundary conditions cannot be set locally: one requires information from both boundaries to set them consistently.

2 Simulations

We conducted simulations to compare the non-local electron heat-flux model with the usual diffusive model. The test case chosen is that used by [20], which is representative of the JET SOL. An ELM crash is simulated by introducing transient sources of heat and particles with duration $200\mu s$ whose spatial distributions are cosines about the centre of the simulation domain. The total ELM energy is 0.4MJ, which is distributed evenly between the ions and electrons, both at the pedestal temperature $T_{ped} = 1.5\text{keV}$. The source region of the SOL is taken to have a width of 10cm, a radius of 3m, a poloidal extent of 2.6m and a field line pitch of $6°$, giving a volume of 4.9m^3 and a parallel extent of $2.6\text{m}/\sin(6°) \approx 25\text{m}$. Explicitly the source terms are

$$S_{ne} = S_{ni} = \begin{cases} \sigma_n \cos\left(\frac{\pi y}{L_s}\right) & |y| < \frac{L_s}{2} \\ 0 & \text{else} \end{cases} \tag{16}$$

$$S_{Ee} = S_{Ei} = \begin{cases} \sigma_E \cos\left(\frac{\pi y}{L_s}\right) & |y| < \frac{L_s}{2} \\ 0 & \text{else} \end{cases} \tag{17}$$

where y is the co-ordinate parallel to the magnetic field with $y = 0$ at the centre of the domain, $L_s = 25\text{m}$ is the length of the source, $\sigma_n \approx 9.1 \times 10^{23}\text{m}^{-3}\text{s}^{-1}$ and
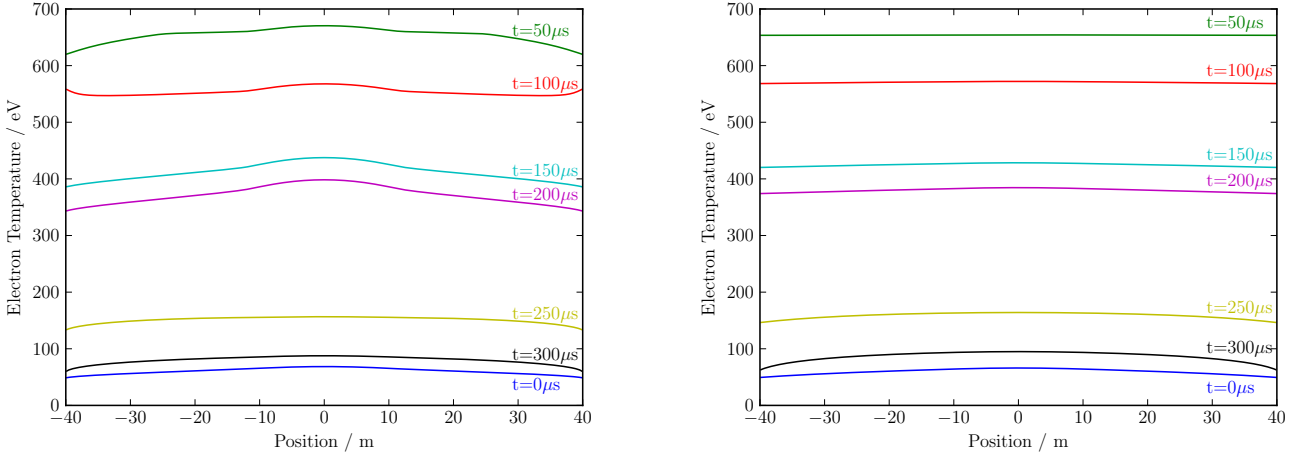
Figure 2: Electron temperature profiles at various times during and after a 200μs ELM using the non-local heat-flux model (left) and a diffusive heat-flux model with a flux limiter of 0.4 (right).
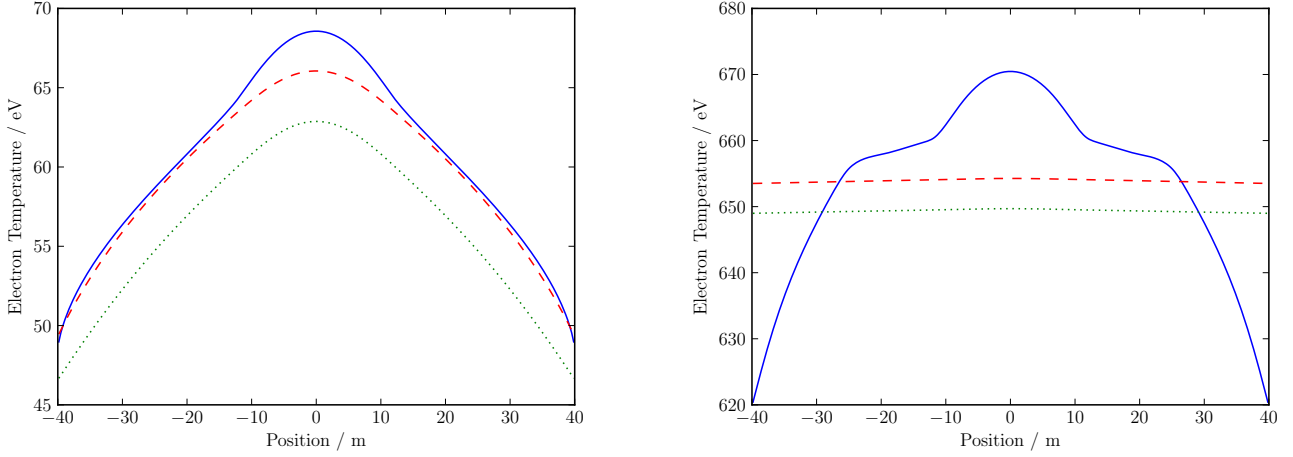

Figure 3: Comparison of the electron temperature profiles from the non-local (solid, blue) and diffusive models with a flux limiter of 0.4 (dashed, red) and without flux limiter (dotted, green): on the left at $t = 0\mu$s (before the ELM) and on the right at $t = 50\mu$s (during the ELM).

$\sigma_E \approx 3.3 \times 10^8 \mathrm{Jm}^{-3}\mathrm{s}^{-1}$. The total length of the domain is 80m. The initial profiles are found by allowing the simulation to relax to a steady state with sources that have similar form but smaller amplitude ($\sigma_n \approx 7.4 \times 10^{22}\mathrm{m}^{-3}\mathrm{s}^{-1}$ and $\sigma_E \approx 4.5 \times 10^6 \mathrm{Jm}^{-3}\mathrm{s}^{-1}$). The ion heat-flux limiter used was $\alpha_i = 0.1$ and the ion viscosity limiter was $b = 0.5$, as indicated by inter-ELM PIC simulations[15]. There are 256 uniformly distributed spatial grid points and a staggered grid is used, with fluxes evaluated at the cell edges.

It has been noted before[3, 20] that the target heat-flux is not strongly affected by kinetic effects, the most important factor being the ions whose transport is mostly convective and therefore well described by fluid models. It is not surprising then that the target heat-flux is similar for the non-local and the diffusive heat-flux models, as shown in Figure 1. One might have thought that using a model which includes kinetic effects on the electron heat-flux would show the rapid response due to fast electrons that is seen in PIC simulations[20]. This is not the case here because both source terms and boundary conditions are given in the fluid picture and do not include kinetic corrections. In order to give a description more fully in agreement with the PIC results some modification of the fluid boundary conditions would also be necessary: in particular the sheath electron heat transmission coefficient shows very strong variation through an ELM[15]. One proposal to achieve this is to use sheath coefficients corresponding to the response to a collisionless Maxwellian wavepacket[23], but this relies on knowledge of the source to derive an explicit time dependence. For three-dimensional simulations where the source on a particular field line is not known in advance, a method which depends only on the fields being evolved is needed. The non-local calculation here depends only on the fluid variables, but derives from them extra information about the non-Maxwellian part of the electron distribution function. It would be interesting to investigate whether this can be put to use in the construction of kinetically-corrected boundary conditions. The conclusion of this is that for one-dimensional studies the non-local electron heat-flux does not by itself offer much improvement with respect to modelling of machine-relevant parameters, which are dominated by the ion dynamics.

The value of the non-local model lies instead in aspects which will be relevant when coupled in to three-dimensional simulations. As shown in Figures 2 and 3 the non-local model has a strong effect on the shape of the electron temperature profiles. The qualitative difference between this non-local model and a flux limiter approach is clear. Before the ELM, a flux limiter with $\alpha_e = 0.4$ is in fairly good agreement with the non-local model, but during the ELM, when the electron temperature is much higher and the collision length is much longer, the same flux limiter cannot sustain temperature gradients of a similar order of magnitude as the non-local model. To do so a much smaller flux limiter would be needed, for example at $t = 50\mu s$ a limiter with $\alpha_e \sim 0.025$ would be required (see Figure 4). A flux limiter cannot be set which is appropriate for the whole range of conditions. This is in agreement with PIC simulations of the SOL[15], which show that to capture the kinetic effects the parameter of a flux limiter model would need to vary both in space and time. In contrast the non-local heat-flux can cover a much broader range of conditions. A PIC simulation of the same sort of ELM (0.4MJ, $200\mu s$) as we have simulated here shows[15, Fig. 7] that the value of the electron heat-flux limiter that would match the kinetic simulation becomes much smaller than the pre-ELM value after $50\mu s$, showing that in the kinetic simulation a much steeper temperature gradient is needed to drive the heat-flux from the source than would be the case with a flux limiter set to the pre-ELM value. Figure 4 shows a similar plot from our non-local heat-flux simulation: the spatial average, $\langle \alpha_e \rangle$, of the flux limiter parameter (here un-normalized, unlike [15, Fig. 7]) that would be needed at each point for the diffusion operator (11) to match the non-local heat-flux. In both cases the minimum value reached by $\langle \alpha_e \rangle$ is similar. [15, Fig. 6] shows that the kinetic correction to the electron sheath heat transmission coefficient, γ_e, passes through 1 (i.e. no correction) at about $60\mu s$, which happens to be the time when $\langle \alpha_e \rangle$ reaches its minimum value. This is why our non-local fluid simulation, which does not include any kinetic corrections to the fluid boundary conditions, is able to find the same value. After $60\mu s$, the fluid heat transmission coefficient is larger than the kinetic one, and so the electrons are cooler in the fluid model, with a corresponding decrease in collision length and increase in $\langle \alpha_e \rangle$. This reemphasizes the importance of developing a better model of the sheath boundary conditions for fluid simulations of the SOL.

One might notice that the $t = 100\mu s$ temperature profile from the non-local model in Figure 2 looks odd: it increases near the boundaries instead of decreasing monotonically from the centre of the domain. The reason is that as the density from the ELM reaches the boundary it causes a temporary glitch while the boundary conditions adjust, with a very steep velocity gradient appearing near the boundary. This causes the convective term in 10 to heat the electrons, resulting in the upturn in temperature. The diffusive model allows enough heat-flux to conduct away this extra heat, but the non-local model does not, which is why this behaviour is noticeable only in the non-local model. The reason for the glitch may be the way the ion viscosity is calculated. A viscosity limiter is needed since without it the viscous heating would increase the temperature of the SOL plasma above the temperature of
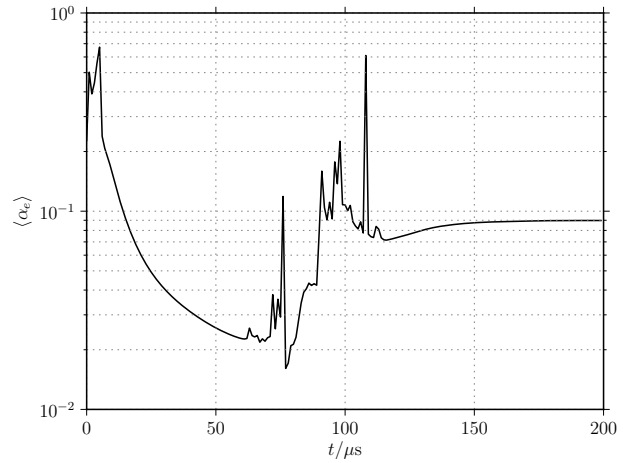

Figure 4: Spatially averaged value of the flux limiter, α_e, that would match the value of the non-local heat-flux.

the source, which is clearly unphysical. On the other hand without some viscosity the velocity of the plasma would increase to above the sound speed. This suggests perhaps that a better method of calculating the viscosity may be useful. It is possible to calculate the ion viscosity in an analogous manner to the calculation of the electron heat-flux used here[24]. The neglect of time derivatives used in this approach is obviously not strictly valid for ions when ELMs occur: the plasma does then evolve significantly on ion timescales. Nevertheless the calculation would be valid both before the ELM begins and in the steady state reached if the ELM continues long enough. It might therefore be reasonably hoped that, while not quantitatively accurate, it would interpolate between the two states in a qualitatively better way than a limiter which can be set only for one or the other state.

2.1 Model Convergence

In the non-local model one can increase the number of moments used; the effect is to extend the validity of the model to longer collision lengths[16], though at the cost of computational speed. The simulations reported here used $L = 20$, $K = 20$ (400 moments). To verify that this number is appropriate, we ran simulations with fewer ($L = 10$, $K = 10$; 100 moments) and more ($L = 40$, $K = 40$; 1600 moments) moments. As shown in Figure 5, the 400 and 1600 moment simulations agree well across the whole range of temperatures in this simulation; they do differ somewhat in the size of their response to the 'glitch' mentioned above but since that is unphysical this difference is not relevant. At the highest temperatures (and hence longest collision lengths) the 100 moment version gives significantly different results.

3 Implementation

The computation of the non-local heat-flux requires many integrals to be calculated: one per moment per field line. Even though the integrand depends on the point of evaluation, it is not necessary to compute separate integrals for each point. The dependence, equation (5), is simple enough that integral at each point can be calculated from
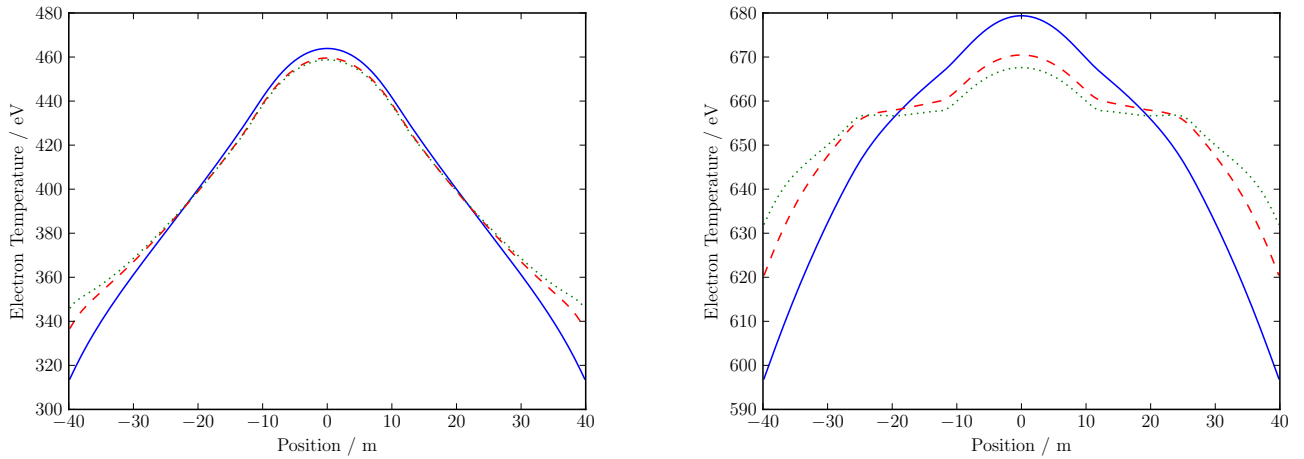
5

Figure 5: Comparison of the electron temperature profiles for 100 (solid, blue), 400 (dashed, red) and 1600 (dotted, green) moment heat-flux models: on the left at $t = 15\mu s$ (as the 100 moment model begins to diverge) and on the right at $t = 50\mu s$ (near the peak electron temperature).

that at the point either to the left or to the right (depending on the sign of the eigenvalue associated with that integral) so that the integrals at every point can be computed in a single loop over the field line. The integrals for different moments and for different field lines are independent, allowing efficient parallelization by overlapping their computations on different processors to minimize idle time. Since this is a one-dimensional, field-parallel calculation, the scaling as the grid is divided in the other directions (i.e. radially and toroidally) is perfect (i.e. linear) since processors dealing with separate field lines do not need to communicate. This favours the division of a three-dimensional simulation grid as finely as possible radially and toroidally before starting to distribute the grid points on a single field line between different processors. However, other operations have diametrically opposed requirements: BOUT++ does not split the simulation grid at all in the toroidal direction in order to allow efficient computation of toroidal Fourier transforms; and perpendicular Laplacian inversions favour splitting of the grid parallel to the field rather than radially[19]. Therefore it is important that this heat-flux calculation scale efficiently when the grid is split in the parallel direction, but with several field lines on each processor. The sub-grid assigned to each processor will have at least as many points as the toroidal size of the grid, and likely several times that: this is the reason that Figure 6 shows the scaling for various numbers of field lines per processor, even though the most efficient splitting for *this* calculation would be to have just one field line per processor. The maximum number of field lines plotted is 64 since, for a grid with 256 parallel points, the evaluation time per grid point for larger numbers of field lines did not change significantly from that for 64. Figure 6 shows that scaling (for a 256 point grid) is near linear up to $16 = \sqrt{256}$ processors, falling to $\sim n^{-0.6}$ above that as the communication time becomes relatively more important. The efficiency (for 64 field lines per processor) at 64 processors, i.e. 4 parallel points per processor, is 56% compared to using a single processor.

The grid for a typical three-dimensional simulation in BOUT++ might have 256 radial, 256 field-parallel and 256 toroidal points; dividing the grid to put 4 radial and 4

parallel points on each processor would mean using 4096 processors. From the point of view just of this parallel heat-flux calculation this means 64 independent sets of 64 processors, with each set having 1028 field lines. As the number of field lines is greater than 64, the efficiency will still be 56% and the total evaluation time (for the heat-flux calculation) for the $256 \times 256 \times 256$ grid will then be $\sim 2.4s$. Including this non-local heat-flux in a three-dimensional simulation will not be detrimental to the scaling performance of BOUT++, and so we anticipate good efficiency up to several thousand processors, as has been previously demonstrated for BOUT++ simulations[19].

The spatial convergence of the calculation compared to a 9192 point grid is shown in Figure 7. 256 point resolution has a root mean square relative error of 4.7×10^{-5}. The input data for the test are some functions chosen to have gradients comparable to the biggest ones found during the ELM simulations (modelled on the $t = 2\mu s$ slice).

4   Conclusions

By using a non-local operator to calculate the electron heat-flux, we can account for some kinetic effects in fluid models, without needing to set parameters by comparison with kinetic simulations or experiment. This is especially beneficial when transients such as ELMs occur because the non-local heat-flux can respond self-consistently to the changing conditions in the plasma in a way that flux limiters cannot.

In one dimensional simulations, the effect on machine-relevant parameters, such as the heat-flux at the divertor targets, is not significant as their behaviour is dominated by the ion dynamics (Figure 1) which, being largely convective, are well described by fluid models.

However, there is a substantial change in the shape of the electron temperature profiles (Figures 2 and 3) which will alter the drive of turbulence in three-dimensional simulations and thus will affect, for example, the width of the strike-point on the divertor. The principal advantage of the technique described here is that it will allow self-consistent three-dimensional simulations: since the
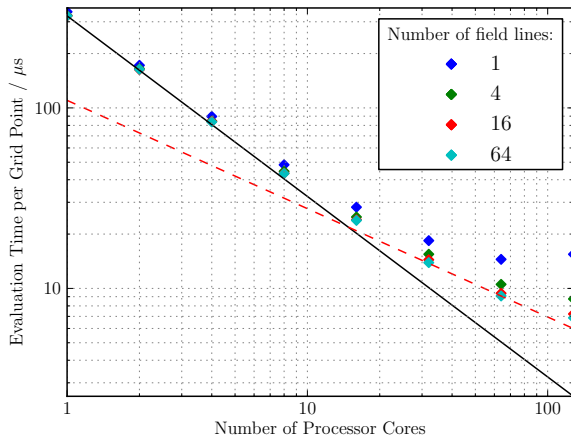
Figure 6: Scaling performance of the non-local heat-flux computation for 400 moments on a 256 point grid on HPC-FF. Extra field lines allow more efficient overlapping of computations, improving the scaling compared to the single field line case. The black, solid line shows linear scaling and the red, dashed line shows $n^{-0.6}$ scaling.
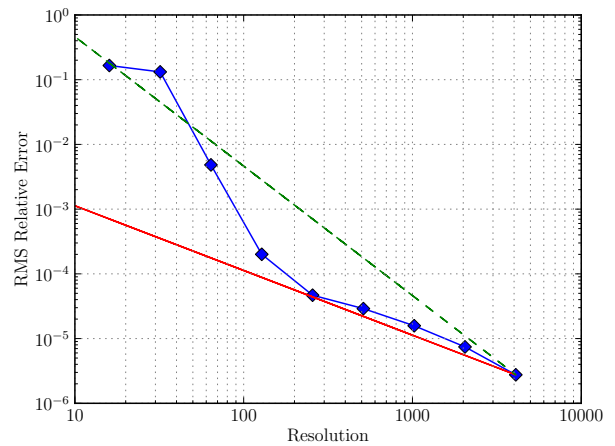

Figure 7: Root-mean-square relative error compared to calculation with 9192 grid points. The red, solid line is $\propto n^{-1}$ and the green, dashed line is $\propto n^{-2}$.

sources of heat and particles on each field line would then be determined by the cross-field transport, achieving a similar effect through flux limiters set by comparison to one-dimensional PIC simulations would be very challenging.

The main limitation preventing a closer match of the electron dynamics between these non-local fluid simulations and PIC simulations such as those in [15] seems to be the response of the sheath-edge boundary conditions to kinetic effects during transients, which have not yet been included in our fluid simulations.

The non-local heat-flux has been implemented in BOUT++ and parallelized efficiently. It is ready to be included in three-dimensional simulations of the SOL.

4.1 Future work

The next step in this work is to move on to three-dimensional turbulence simulations of the SOL, to investigate the effects on turbulence and perpendicular transport of the electron temperature gradients seen here that are missed by local heat-fluxes currently used in SOL fluid models.

In order to correctly describe realistic tokamak geometries, the model should be extended to include the effects of ∇B on the heat-flux calculation. The effect will be to add an additional drive term to equation (1) which, as it depends only on the Maxwellian part of the distribution function, should add only a modest amount of additional complication.

In the non-local approach one has more information about the electron distribution function than just the density and temperature. It may be possible to use this information to improve the modelling of the sheath and so find more accurate boundary conditions for SOL fluid models. Whether by this method or another, finding a way to include some kinetic corrections to the sheath transmission coefficients would greatly improve the accuracy of

fluid descriptions of parallel transport in the SOL.

Since convection dominates over conduction for the ions, kinetic corrections are less important; flux and viscosity limiters describe the behaviour of the ions better than is the case for the electrons. There may however be some scope for improvement in this area from application of a non-local model to the ion dynamics also. The variation of the ion viscosity limiter (inferred from a PIC simulation) through an ELM crash is not as dramatic as that of the electron heat-flux limiter[15]. However, the value of the viscosity limiter does have a significant effect on the dynamics, affecting in particular the speed reached by the plasma and hence the time for the ELM to reach the target. Though a non-local calculation on the same lines as that used here for the electron heat-flux[24] is not guaranteed to be valid for the ion dynamics due to the neglect of time derivatives, it seems worth investigating whether it might be able to give a better qualitative agreement with kinetic simulations and therefore be of use for improving fluid turbulence simulations.

Acknowledgements

References

[1] A. Loarte, B. Lipschultz, A.S. Kukushkin, G.F. Matthews, P.C. Stangeby, N. Asakura, G.F. Counsell, G. Federici, et al. Chapter 4: Power and particle control. *Nuclear Fusion*, 47(6):S203, 2007. URL http://stacks.iop.org/0029-5515/47/i=6/a=S04.

[2] A. Loarte, M. Sugihara, M. Shimada, A. Kukushkin, D. Campbell, et al. Iter elm control requirements, elm control schemes & required r&d. In *Proceedings of 23rd IAEA Fusion Energy Conference*, 2010.

[3] R.A. Pitts, P. Andrew, G. Arnoux, T. Eich, W. Fundamenski, A. Huber, C. Silva, D. Tskhakaya, and JET EFDA Contributors. Elm transport in the jet scrape-off layer. *Nuclear Fusion*, 47(11):1437, 2007. URL http://stacks.iop.org/0029-5515/47/i=11/a=005.

[4] D.A. D'Ippolito, J.R. Myra, and S.J. Zweben. Convective transport by intermittent blob-filaments: Comparison of theory and experiment. *Physics of Plasmas*, 18(6):060501, 2011. doi: 10.1063/1.3594609. URL http://link.aip.org/link/?PHP/18/060501/1.

[5] J.R. Myra, D.A. Russell, D.A. D'Ippolito, J.-W. Ahn, R.Maingi, R.J. Maqueda, D.P. Lundberg, D.P. Stotler, et al. Reduced model simulations of the scrape-off-layer heat-flux width and comparison with experiment. *Physics of Plasmas*, 18(1):012305, 2011. doi: 10.1063/1.3526676. URL http://link.aip.org/link/?PHP/18/012305/1.

[6] F. Militello, W. Fundamenski, V. Naulin, and A.H. Nielsen. Simulations of edge and scrape off layer turbulence in mega ampere spherical tokamak plasmas. *Plasma Physics and Controlled Fusion*, 54(9):095011, 2012. URL http://stacks.iop.org/0741-3335/54/i=9/a=095011.

[7] O.E. Garcia, V. Naulin, A.H. Nielsen, and J. Juul Rasmussen. Computations of intermittent transport in scrape-off layer plasmas. *Phys. Rev. Lett.*, 92: 165003, Apr 2004. doi: 10.1103/PhysRevLett.92. 165003. URL http://link.aps.org/doi/10.1103/PhysRevLett.92.165003.

[8] O.E. Garcia, N.H. Bian, and W. Fundamenski. Radial interchange motions of plasma filaments. *Physics of Plasmas*, 13(8):082309, 2006. doi: 10.1063/1.2336422. URL http://link.aip.org/link/?PHP/13/082309/1.

[9] G.Q. Yu, S.I. Krasheninnikov, and P.N. Guzdar. Two-dimensional modelling of blob dynamics in tokamak edge plasmas. *Physics of Plasmas*, 13(4):042508, 2006. doi: 10.1063/1.2193087. URL http://link.aip.org/link/?PHP/13/042508/1.

[10] D.A. Russell, J.R. Myra, and D.A. D'Ippolito. Saturation mechanisms for edge turbulence. *Physics of Plasmas*, 16(12):122304, 2009. doi: 10.1063/1.3270051. URL http://link.aip.org/link/?PHP/16/122304/1.

[11] J. Madsen, O.E. Garcia, J. Staerk Larsen, V. Naulin, A.H. Nielsen, and J. Juul Rasmussen. The influence of finite larmor radius effects on the radial interchange motions of plasma filaments. *Physics of Plasmas*, 18(11):112504, 2011. doi: 10.1063/1.3658033. URL http://link.aip.org/link/?PHP/18/112504/1.

[12] P. Ricci, F.D. Halpern, S. Jolliet, J. Loizu, A. Mosetto, A. Fasoli, I. Furno, and C. Theiler. Simulation of plasma turbulence in scrape-off layer conditions: the gbs code, simulation results and code validation. *Plasma Physics and Controlled Fusion*, 54 (12):124047, 2012. URL http://stacks.iop.org/0741-3335/54/i=12/a=124047.

[13] J.R. Angus, M.V. Umansky, and S.I. Krasheninnikov. Effect of drift waves on plasma blob dynamics. *Phys. Rev. Lett.*, 108:215002, May 2012. doi: 10.1103/PhysRevLett.108.215002. URL http://link.aps.org/doi/10.1103/PhysRevLett.108.215002.

[14] J.R. Angus, M. Umansky, and S.I. Krasheninnikov. 3d blob modelling with bout++. *Contributions to Plasma Physics*, 52(5-6):348–352, 2012. ISSN 1521-3986. doi: 10.1002/ctpp.201210015. URL http://dx.doi.org/10.1002/ctpp.201210015.

[15] D. Tskhakaya, F. Subba, X. Bonnin, D.P. Coster, W. Fundamenski, R.A. Pitts, and JET EFDA Contributors. On kinetic effects during parallel transport in the sol. *Contributions to Plasma Physics*, 48(1-3):89–93, 2008. ISSN 1521-3986. doi: 10.1002/ctpp.200810015. URL http://dx.doi.org/10.1002/ctpp.200810015.

[16] J.Y. Ji, E.D. Held, and C.R. Sovinec. Moment approach to deriving parallel heat flow for general collisionality. *Physics of Plasmas*, 16(2):022312, 2009. doi: 10.1063/1.3079072. URL http://link.aip.org/link/?PHP/16/022312/1.

[17] J.F. Luciani, P. Mora, and J. Virmont. Nonlocal heat transport due to steep temperature gradients. *Phys. Rev. Lett.*, 51:1664–1667, Oct 1983. doi: 10.1103/PhysRevLett.51.1664. URL http://link.aps.org/doi/10.1103/PhysRevLett.51.1664.

[18] O.V. Batishchev, V.Yu. Bychenkov, F. Detering, W. Rozmus, R. Sydora, C.E. Capjack, and V.N. Novikov. Heat transport and electron distribution function in laser produced plasmas with hot spots. *Physics of Plasmas*, 9(5):2302–2310, 2002. doi: 10.1063/1.1461385. URL http://link.aip.org/link/?PHP/9/2302/1.

[19] B.D. Dudson, M.V. Umansky, X.Q. Xu, P.B. Snyder, and H.R. Wilson. BOUT++: A framework for parallel plasma fluid simulations. *Computer Physics Communications*, 180:1467–1480, 2009. ISSN 0010-4655. doi: DOI:10.1016/j.cpc.2009.03.008. URL http://www.sciencedirect.com/science/article/B6TJ5-4VTCM95-3/2/ed200cd23916d02f86fda4ce6887d798.

[20] E. Havlíčková, W. Fundamenski, D. Tskhakaya, G. Manfredi, and D. Moulton. Comparison of fluid and kinetic models of target energy fluxes during edge localized modes. *Plasma Physics and Controlled Fusion*, 54(4):045002, 2012. URL http://stacks.iop.org/0741-3335/54/i=4/a=045002.

[21] J.Y. Ji and E.D. Held. Exact linearized coulomb collision operator in the moment expansion. *Physics of Plasmas*, 13(10):102103, 2006. doi: 10.1063/1.2356320. URL http://link.aip.org/link/?PHP/13/102103/1.

[22] P.C. Stangeby. *The plasma boundary of magnetic fusion devices*. Institute of Physics Pub., 2000.

[23] W. Fundamenski, R.A. Pitts, and JET EFDA contributors. A model of elm filament energy evolution due to parallel losses. *Plasma Physics and Controlled Fusion*, 48(1):109, 2006. URL http://stacks.iop.org/0741-3335/48/i=1/a=008.

[24] J.Y. Ji and E.D. Held. Moment approach to deriving a unified parallel viscous stress in magnetized plasmas. *Journal of Fusion Energy*, 28: 170–174, 2009. ISSN 0164-0313. doi: 10.1007/s10894-008-9169-7. URL http://dx.doi.org/10.1007/s10894-008-9169-7.